An *ABCA4* loss-of-function mutation causes a canine form of Stargardt disease

Suvi Mäkeläinen[1], Marta Gòdia[1,#a], Minas Hellsand[2], Agnese Viluma[1], Daniela Hahn[1], Karim Makdoumi[3], Caroline J. Zeiss[4], Cathryn Mellersh[5], Sally L. Ricketts[5], Kristina Narfström[6], Finn Hallböök[2], Björn Ekesten[7], Göran Andersson[1], Tomas F. Bergström[1*]

[1]Department of Animal Breeding and Genetics, Swedish University of Agricultural Sciences, Uppsala, Sweden

[2]Department of Neuroscience, Uppsala University, Uppsala, Sweden

[3]Department of Ophthalmology, Faculty of Medicine and Health, Örebro University, Sweden

[4]Yale University School of Medicine, New Haven, Connecticut, United States of America

[5]Canine Genetics Research Group, Kennel Club Genetics Centre, Animal Health Trust, Lanwades Park, Kentford, Newmarket, Suffolk, United Kingdom

[6]Section for Comparative Ophthalmology, College of Veterinary Medicine, University of Missouri-Columbia. Missouri, United States of America

[7]Department of Clinical Sciences, Swedish University of Agricultural Sciences, Uppsala, Sweden

[#a]Current Address: Department of Animal Genomics, Centre for Research in Agricultural Genomics (CRAG) CSIC-IRTA-UAB-UB, Campus UAB, Bellaterra, Spain

*Corresponding author

E-mail: tomas.bergstrom@slu.se (TB)

Abstract

Autosomal recessive retinal degenerative diseases cause visual impairment and blindness in humans and dogs. Currently, no standard treatment is available but pioneering gene therapy-based canine models have been instrumental for clinical trials in humans. To study a novel form of retinal degeneration in Labrador retriever dogs with clinical signs indicating cone and rod degeneration, we used whole-genome sequencing of an affected sib-pair and their unaffected parents. A frameshift insertion in the ATP binding cassette subfamily A member 4 (*ABCA4*) gene (c.4176insC), leading to a premature stop codon in exon 28 (p.F1393Lfs1395) was identified. In contrast to unaffected dogs, no full-length ABCA4 protein was detected in the retina of an affected dog. The *ABCA4* gene encodes a membrane transporter protein localized in the outer segments of rod and cone photoreceptors. In humans, the *ABCA4* gene is associated with Stargardt disease (STGD), an autosomal recessive retinal degeneration leading to central visual impairment. A hallmark of STGD is the accumulation of lipofuscin deposits in the retinal pigment epithelium. The discovery of a canine homozygous *ABCA4* loss-of-function mutation may advance the development of dog as a large animal model for human STGD.

Author summary

Stargardt disease (STGD) is the most common inherited retinal disease causing visual impairment and blindness in children and young adults, affecting 1 in 8-10 thousand people. For other inherited retinal diseases, the dog has become an established comparative animal model, both for identifying the underlying genetic causes and for developing new treatment methods.

To date, there is no standard treatment for STGD and the mouse model is the only available animal model to study the disease. As a nocturnal animal, the morphology of the mouse eye differs from humans and therefore the mouse model is not ideal for developing methods for treatment. We have studied a novel form of retinal degeneration in Labrador retrievers showing clinical signs similar to human STGD. To investigate the genetic cause of the disease, we used whole-genome sequencing of a family quartet including two affected offspring and their unaffected parents. This led to the identification of a loss-of-function mutation in the *ABCA4* gene. The findings of this study may enable the development of a canine model for human STGD.

Introduction

Inherited retinal dystrophies are a genetically and clinically heterogeneous group of eye diseases leading to severe visual impairment in both humans and dogs [1-7]. These diseases include various forms of retinitis pigmentosa (RP), Leber congenital amaurosis (LCA), age-related macular degeneration (AMD), cone-rod dystrophies (CRD), and Stargardt disease (STGD) and are caused by many different mutations leading to deterioration of neuroretinal and retinal pigment epithelial (RPE) function. Over 100 years ago, progressive retinal atrophy (PRA) was described as a canine equivalent of human RP [8] and is today the most common inherited retinal degenerative disease in dogs [9]. The shared phenotypic similarity of inherited retinal dystrophies in dogs and humans has made canine models attractive for gene discovery and for experimental treatments, including gene therapy, of inherited degenerative retinal disease [1, 7, 10-13]. The development of gene therapy for *RPE65*-mediated LCA is an example where a canine comparative model has been instrumental for proof-of-principle trials [10, 11, 14-16]. The identification of the p.C2Y mutation (OMIM: 610598.0001) in the *PRCD* gene is another illustrative example of the benefits of using

canine genetics to find homologous candidate genes for human retinal dystrophies; the *PRCD* gene was initially mapped and identified in PRA affected dogs and subsequently in a human family with RP [17]. This mutation segregates in multiple dog breeds, including the Labrador retriever, where no other causative genetic variants for inherited retinal degenerations have been identified. In this study, a Labrador retriever sib-pair, one male and one female, negative for the p.C2Y mutation, was diagnosed with a novel form of retinal disease. To identify genetic variants associated with this novel canine retinal disease, we performed whole-genome sequencing (WGS) of the two affected individuals and their unaffected parents.

Results and discussion

The affected dogs were visually impaired under both daylight and dim light conditions. Ophthalmoscopy revealed abnormal mottling of both central and peripheral retina, reduced reflection of light, as well as subtle retinal vascular attenuation (**Fig 1a**). A patchy outer retinal atrophy was observed with optical coherence tomography (OCT) (**Fig 1b**). In contrast, retinal layering and thickness of both outer and inner retinal layers appeared similar in an unaffected dog and a carrier (**Fig 1b**). Compared to a retina of a normal dog (**Fig 1c)**, loss of cones, less densely packed photoreceptor nuclei, increased lipofuscin accumulation in the RPE, as well as multifocal RPE hyperplasia and hypertrophy with focal atrophy of the overlying neuroretina were observed with light-microscopy in the affected male (**Fig 1d**). We used flash-electroretinography (FERG) to study the photoreceptor function in the three dogs. The inclination of the first part of the a-waves of the dark-adapted FERG in response to a bright flash was less steep and the amplitude of the a-waves were lower in both a carrier and an affected dog compared to the age-matched unaffected dog (**Fig 1e**). The a-wave of the affected dog is widened with longer implicit time. Furthermore, oscillatory potentials are less

conspicuous and the first part of the b-wave is essentially lost (**Fig 1e**). Light-adapted cone transient responses (**Fig 1f**) and cone flicker (**Fig 1g**) were profoundly abnormal in the affected dog, but considerably closer to normal in the carrier. In summary, FERG demonstrated loss of cone function and abnormal rod responses, including abnormally slow dark-adaptation in the affected dog (**Fig 1e-g**). Taken together, clinical features were atypical for PRA, but showed similarities to human STGD.

The WGS of the family quartet resulted in an average coverage of 18.2x (**S1 Table**) and the identification of 6.0 x 10^6 single nucleotide variants (SNVs) and 1.9 x 10^6 insertions/deletions (INDELs), of which 48,299 SNVs and 5,289 INDELs were exonic. We used conditional filtering to identify 322 SNVs (of which 117 were nonsynonymous) and 21 INDELs that were consistent with an autosomal recessive pattern of inheritance (**S2 Table**). To further reduce the number of candidate variants, we compared the positions of the variants to 23 additional dog genome sequences to identify 18 nonsynonymous SNVs in 13 different genes and four INDELs in four genes that were private to the Labrador retriever family (**S2 and S3 Tables**). Fourteen of these genes were not strong candidates based on reported function and predicted effect and were not considered further. The remaining three genes, *KIAA1549*, Usherin *(USH2A),* and ATP binding cassette subfamily A member 4 (*ABCA4)* are listed in the Retinal Information Network (RetNet) database as associated with human retinal diseases and thus considered as causative candidates for canine retinal degeneration[18]. However, the variant at the *KIAA1549* gene was predicted to have a neutral effect on the protein structure (PROVEAN score -2.333, Polyphen-2 score 0.065) and was therefore discarded. The genetic variants in the *USH2A* (exon 43; c.7244C>T) and *ABCA4* (exon 28; c.4176insC) genes were validated by Sanger sequencing. Mutations in the *USH2A* gene are associated with Usher syndrome and RP, resulting in hearing loss and visual impairment [19]. The identified

125 nonsynonymous substitution in the *USH2A* was scored as "probably damaging" using
126 Polyphen-2 (score of 0.97) and as "deleterious" using PROVEAN (score of -4.933) (**S3**
127 **Table**). Next, we evaluated if the genetic variants of *USH2A* and *ABCA4* were concordant
128 with the disease by genotyping eight additional clinically affected and thirteen unaffected
129 Labradors. Out of these dogs, 16 were related to the family quartet used in the WGS (**S1 Fig**).
130 The *USH2A* variant was discordant with the disease phenotype and was therefore excluded
131 from further analysis (**S4 Table**). In contrast, all eight affected individuals were homozygous
132 for the *ABCA4* insertion and the 13 unaffected individuals were either heterozygous or
133 homozygous for the wild-type allele (**S4 Table**).
134
135 In the *ABCA4* gene, we identified a single base pair insertion of a cytosine (C) in a cytosine
136 mononucleotide-repeat region in exon 28, where the canine reference sequence consists of
137 seven cytosines (CanFam3.1 Chr6:55,146,549-55,146,555) (**Fig 2a**). The insertion in this
138 region results in a non-synonymous substitution at the first codon downstream of the repeat
139 (c.4176insC), and subsequently leads to a premature stop codon (p.F1393Lfs*1395) (**Fig 2c**).
140 If translated, this would result in a truncation of the last 873 amino acids of the wild-type
141 ABCA4 protein (**Fig 2b-c)**. Both the human and the dog *ABCA4* gene consists of 50 exons
142 and encodes a ~250 kDa ABC transporter protein (**Fig 2d**) (human and dog ABCA4 consists
143 of 2,273 and 2,269 amino acid residues, respectively) [20, 21]. ABCA4 is localized to the
144 disc membranes of photoreceptor outer segments and facilitates the clearance of all-*trans*-
145 retinal from the photoreceptor discs [22-24].
146
147 To compare retinal *ABCA4* gene expression in an affected, a carrier, and a wild-type dog, we
148 performed quantitative RT-PCR (qPCR). Primers were designed to amplify three different
149 regions of the gene. The amplicons spanned the 5´-end (exons 2-3), the identified insertion

(exons 27-28) and the 3´-end of the *ABCA4* gene (exons 47-48) (**S5 Table**). Each of the three primer pairs amplified a product of expected size in all three individuals. This suggests that despite the insertion leading to a premature stop codon in exon 28, the transcripts are correctly spliced. Relative levels of *ABCA4* mRNA were lower for the allele with the insertion in comparison to the wild-type allele (**Fig 3a**). This is consistent with nonsense-mediated decay (NMD) degrading a fraction of the transcripts with premature translation stop codon [25]. Transcripts not targeted by NMD could potentially be translated into a truncated protein of only 1,394 amino acid residues including the first extracellular domain (ECD1), the first nucleotide-binding domain (NBD1) and two membrane-spanning regions (**Fig 2b**) but lacking the second extracellular domain (ECD2) and the second nucleotide-binding domain (NBD2) [26-28] (**Fig 2b-d**). The NBDs are conserved across species and the NBD2, which is also referred to as the ATP binding cassette of the ABCA4 protein, has been shown to be particularly critical for its function as a flippase [26, 28].

To investigate the presence of full-length protein, we performed western blot analysis using an anti-ABCA4 antibody recognizing a C-terminal epitope and detecting a protein product with an approximate size of ~250 kDa. We observed a single, correctly-sized band in samples prepared from both wild-type and heterozygous dogs. The intensity of staining in retinal protein samples from the heterozygous individual was markedly lower in comparison to the samples from the wild-type retina (**Fig 3b**). In contrast, no band was detected in the retinal sample from the affected dog. To confirm the presence of photoreceptor cells, we used an anti-RHO antibody and detected similar levels of rhodopsin in all three samples (**Fig 3b**). These results suggest that no full-length protein product is produced as a result of the insertion leading to a frameshift and a premature stop codon.

175 Fluorescence histochemistry was used to analyze the ABCA4 protein expression and peanut
176 agglutinin (PNA)-binding in retinas from three dogs with different *ABCA4* genotypes. PNA
177 binds selectively to cones in the retina[29]. ABCA4 immunoreactivity (IR) was seen in the
178 outer part of the neural retina and the RPE. The pattern corresponded to photoreceptor outer
179 segments and overlapped partially with the PNA label. PNA stained cone-shaped cells
180 spanning both the inner and outer segments (**Fig 4a**). ABCA4 IR was also seen on PNA-
181 negative outer segments, likely to be rod photoreceptors and RPE. The ABCA4 IR and PNA
182 patterns were similar in wild-type and heterozygous retinas. In sharp contrast, no ABCA4 IR
183 was found in the affected retina (**Fig 4a-c**). In addition, no evident PNA-staining was
184 observed, implying loss of cones. We therefore counted photoreceptor nuclei in the three
185 genotypes and compared the outer and inner nuclear layers. The photoreceptor nuclei are
186 positioned in the outer nuclear layer but not in the inner nuclear layer and there were fewer
187 nuclei in the affected outer nuclear layer in the affected retina than in the wild-type or
188 heterozygous retina (**Fig 4d**). The corresponding reduction of nuclei was not seen in the inner
189 nuclear layer, suggesting that photoreceptors were affected but not neurons in the inner
190 nuclear layer. The loss of ABCA4 protein, loss of cone outer segment-PNA-staining, and the
191 reduction of photoreceptor nuclei in the affected retina strongly imply that photoreceptors
192 degenerate in the ABCA4$^{-/-}$ retina.
193
194 The RPE layer of the affected retina was autofluorescent (**Fig 4c**), indicating accumulation of
195 lipofuscin[30]. We analyzed autofluorescence in RPE from retinas of three dogs with
196 different *ABCA4* genotypes. The autofluorescence in the affected retina was higher than in
197 that of the retinas in the other genotypes (**Fig 4g-h)**. The higher autofluorescence indicates an
198 increased accumulation of lipofuscin in the affected retina compared to the retinas from wild-
199 type or heterozygous individuals.

The ABCA4 protein functions as an ATP-dependent flippase in the visual cycle, transporting *N*-retinylidene-phophatidylethanolamine (*N*-Ret-PE) from the photoreceptor disc lumen to the cytoplasmic side of the disc membrane [31, 32]. *N*-Ret-PE is a reversible adduct spontaneously formed between all-*trans*-retinal and phophatidylethanolamine (PE), and is unable to diffuse across the membrane by itself. Once transported by ABCA4, *N*-Ret-PE is dissociated and all-*trans*-retinal will re-enter to the visual cycle [33]. Defective ABCA4 leads to accumulation of *N*-Ret-PE, which together with all-*trans*-retinal, will form di-retinoid-pyridinium-phosphatidylethanolamine (A2PE) that is further hydrolyzed to phosphatidic acid (PA) and a toxic bis-retinoid, di-retinal-pyridinium-ethanolamine (A2E) [34]. This will lead to an accumulation of A2E in RPE cells when photoreceptor discs are circadially shed and phagocytosed by the RPE [35-37]. A2E is a major component of RPE lipofuscin, accounts for a substantial portion of its autofluorescence, and has a potentially toxic effect on the RPE leading to photoreceptor degeneration [35, 38-40]. In ABCA4-mediated diseases, cone photoreceptors are typically affected prior to rods [41]. The accumulation of lipofuscin and the degeneration of cones seen in this study of Labrador retrievers are also characteristic of STGD in humans [30, 42].

Mutations in the human *ABCA4* (*ABCR*) gene cause autosomal recessive STGD, autosomal recessive forms of CRD and RP [43-45]. The gene was first cloned and characterized in 1997 [20], and 873 missense and 58 loss-of-function variants have been reported in the ExAC database [46, 47], many of which are associated with visual impairment [48-50]. Currently, there is no standard treatment for STGD in humans and *Abca4*$^{-/-}$ mouse is the only available animal model [51, 52]. Mice, however, lack the macula, which is primarily the area affected in STGD, and although mouse models have provided insight into genesis of the lipofuscin

fluorophore A2E, *Abca4*$^{-/-}$ mice do not exhibit a significant retinal degeneration phenotype [53, 54]. Unlike the mouse retina, the dog has a cone rich fovea-like area functionally similar to human fovea centralis [1, 3, 11]. The canine eye is also similar in size to the human eye, and dog has successfully been used for experimental gene therapy for retinal degenerations such as LCA, RP, rod-cone dysplasia type 1 (rcd1) [12, 16, 55]. For over a decade there has been interest in finding a canine model for *ABCA4* mediated diseases [56-58]. The loss-of-function mutation identified here can be used to develop large animal model for human STGD.

Methods

Animals and samples

A family quartet of Labrador retrievers (sire, dam, and two affected offspring numbered LAB1, LAB2, LAB3 and LAB4 respectively) were used in the whole-genome sequencing (WGS). In addition, 16 related individuals (LAB5 to LAB20, see **S1 Figure**) as well as five unrelated Labradors (LAB 21 to LAB25) were used to validate the WGS findings. Whole blood samples from these dogs were collected in EDTA tubes and genomic DNA was extracted using 1 ml blood on a QIAsymphony SP instrument and the QIAsymphony DSP DNA Kit (Qiagen). We obtained eyes from the affected male (LAB4) and his unaffected sibling (LAB6) at the age of 12, as well as from one unrelated, unaffected 11-year-old female Labrador retriever (LAB24) and one 10-year-old male German spaniel (GS) after their euthanization (with sodium pentobarbithal (Pentobarbithal 100 mg/ml, Apoteket Produktion & Laboratorier AB) for unrelated reasons. All samples were obtained with informed dog owner consent. Ethical approval was granted by the regional animal ethics committee (Uppsala djursförsöksetiska nämd; Dnr C12/15).

Ophthalmic exam and optical coherence tomography (OCT)

Ophthalmic examination included reflex testing, testing of vision with falling cotton balls under dim and daylight conditions, indirect ophthalmoscopy and slit-lamp biomicroscopy. The affected male (LAB4), his unaffected sibling (LAB6) and an unaffected, age-matched, female Labrador (LAB22) were examined with spectral-domain OCT (Topcon 3D OCT-2000, Topcon Corp.). The examination was done after pupillary dilation, but without sedation, using repeated horizontal single line scans (6 mm, 1024 A-scans) (Topcon 3D OCT-2000, Topcon Corp.) along the visual streak area.

Flash-electroretinography (FERG)

We recorded FERG bilaterally from the three dogs examined with OCT under general anaesthesia. Sedation with intramuscular acepromazine 0.03 mg/kg (Plegicil vet., Pharmaxim Sweden AB) was followed by induction with propofol 10 mg/kg IV (Propovet, Orion Pharma Animal Health AB). After intubation, inhalation anaesthesia was maintained with isoflurane (Isoflo vet., Orion Pharma Animal Health AB). Corneal electrodes (ERG-JET, Cephalon A/S) were used with isotonic eye drops (Comfort Shield, i.com medical GmbH) as coupling agent. Gold plated, cutaneous electrodes served as ground and reference electrodes (Grass, Natus Neurology Inc.) at the vertex and approximately 3 cm caudal to the lateral canthi, respectively. Light stimulation, calibration of lights and processing of signals were performed as described by Karlstam et al., 2011[59]. We used a slightly modified ECVO protocol[60], where the process of dark-adaptation was monitored for 1 hour before a dark-adapted response intensity series was performed.

Histopathology

Sectioned eyes from the affected male (LAB4) and the unaffected male GS were immersed in Davidson's Solution. The eyes were dehydrated in ethanol, paraffin embedded, cut into 4 µm thick sections and stained with haematoxylin and eosin (H&E).

Whole-genome sequencing

Genomic DNA from four Labrador retriever dogs (LAB1, LAB2, LAB3 and LAB4) was fragmented using the Covaris M220 instrument (Covaris Inc.), according to the manufacturer's instructions. To obtain sufficient sequence depth, we constructed two biological replicates of libraries with insert sizes of 350 bp and 550 bp following TruSeq DNA PCR-Free Library Prep protocol. The libraries were multiplexed and sequenced on a NextSeq500 instrument (Illumina) for 100 x 2 and 150 x 2 cycles using the High Output Kit and High Output Kit v2, respectively. The raw base calls were de-multiplexed and converted to fastq files using bcl2fastq v.2.15.0 (Illumina). The two sequencing runs from each individual were merged, trimmed for adapters and low-quality bases using Trimmomatic v.0.32[61], and aligned to the canine reference genome CanFam3.1 using Burrows-Wheeler Aligner (BWA) v.0.7.8[62]. Aligned reads were sorted and indexed using Samtools v.1.3[63] and duplicates were marked using Picard v.2.0.1. The BAM files were realigned and recalibrated with GATK v.3.7[64]. Multi-sample variant calling was done following GATK Best Practices [65] using publicly available genetic variation Ensembl Variation Release 88 in dogs (*Canis lupus familiaris*). We filtered the variants found by GATK using the default values defining two groups of analyses: trio 1 and 2, both consisting of the same sire and dam, and one of their affected offspring. Variants annotated in the exonic region with ANNOVAR v.2017.07.16 [66], presenting an autosomal recessive inheritance pattern and shared between the two trios were selected for further evaluation. To predict the effects of amino acid changes on protein function, we evaluated SNVs using PolyPhen-2 v2.2.2r398

299 [67] and PROVEAN v.1.1.3 [68] and nonframeshift INDELS using PROVEAN v.1.1.3.
300 Frameshift INDELs were manually inspected using The Integrative Genomics Viewer (IGV)
301 [69, 70]. The sequence data were submitted to the European Nucleotide Archive with the
302 accession number PRJEB26319.
303
304 **Validation of the variants**
305 To validate the WGS results, we designed primers amplifying the variants c.7244C>T in
306 *USH2A* gene and c.4176insC in *ABCA4* gene with Primer3 [71, 72] (**S5 Table**) and
307 sequenced the family quartet using Applied Biosystems 3500 Series Genetic Analyzer
308 (Applied Biosystems, Thermo Fisher Scientific). To test if the variants were concordant with
309 the disease, 21 additional ophthalmologically evaluated Labrador retrievers were genotyped
310 by Sanger sequencing. Eight of these dogs were clinically affected and thirteen showed no
311 signs of retinal degeneration by the age of seven years.
312
313 **Quantitative RT-PCR (qPCR)**
314 Neuroretinal samples were collected from the affected dog (LAB4), the heterozygous sibling
315 (LAB6), and the unaffected female (LAB24). The samples were immediately preserved in
316 RNAlater (SigmaAldrich), homogenized with Precellys homogenizer (Bertin Instruments)
317 and total RNA was extracted with RNAeasy mini kit (Qiagen) according to the
318 manufacturer's instructions. RNA integrity and quality were inspected with Agilent 6000
319 RNA Nano kit with the Agilent 2100 Bioanalyzer system (Agilent Technologies). cDNA was
320 synthesized using RT^2 First Strand kit (Qiagen) with random hexamers provided in the kit.
321 cDNA concentration was inspected with Qubit ssDNA Assay kit (Life Technologies). RT^2
322 qPCR Primer Assay (Qiagen) was used to amplify the reference gene *GAPDH*. To amplify
323 the target gene *ABCA4*, we designed custom primers with Primer3 [71, 72] targeting three

different regions spanning exons 2 to 3, 27 to 28, and 47 to 48 (**S5 Table**). We amplified the cDNA fragments encoding regions of interest using RT^2 SYBR Green ROX qPCR Mastermix (Qiagen) with StepOnePlus Real-Time PCR system (Applied Biosystems, Thermo Fisher Scientific), according to the manufacturer's instructions. Target gene expression was normalized to expression of *GAPDH*, and shown relative to a control *ABCA4*$^{+/+}$ sample ($\triangle\triangle C_T$ method). The results were confirmed in two independent experiments.

SDS-Gel Electrophoresis and Western Blotting

We extracted protein from the neuroretinal samples of the individuals used in qPCR (see above) by homogenization in Pierce RIPA lysis buffer (Thermo Scientific) supplemented with phosphatase inhibitor cocktail (Sigma, P8340) using the Precellys homogenizer (Bertin Instruments). Protein concentration was determined using the Pierce BSA Protein Assay kit (Thermo Fischer Scientific). 50 µg of protein samples were resolved by SDS-PAGE, transferred to nitrocellulose membrane, and immunoblotted with the following primary antibodies: ABCA4 (Novus Biologicals, NBP1-30032, 1:1000), GAPDH (Thermo Scientific, MA5-15738, 1:1000), Rhodopsin (Novus Biologicals, NBP2-25160SS, 1:5000), followed by Anti-Mouse IgG horseradish peroxidase-conjugated secondary antibody (R&D Systems, HAF007, 1:5000). Binding was detected using the Clarity western ECL substrate (Bio-Rad).

Fluorescence histochemistry

Tapetal fundus from the affected male (LAB4), his heterozygous sibling (LAB6), and the unaffected GS were fixed in 4% PFA in 1x PBS on ice for 15 minutes, washed in 1x PBS for 10 minutes on ice, and cryoprotected in 30% sucrose overnight at 4°C. The central part of the fundus was embedded in Neg-50™ frozen section medium (Thermo Scientific), and 10 µm

sections were collected on Superfrost Plus slides (J1800AMNZ, Menzel-Gläser). The sections were re-hydrated in 1x PBS for 10 minutes, incubated in blocking solution (1% donkey serum, 0.02% thimerosal, and 0.1% Triton X-100 in 1x PBS) for 30 minutes at room temperature, and incubated in primary antibody ABCA4 (1:500, NBP1-30032, Novus Biologicals) and FITC-conjugated lectin PNA (1:400, L21409, Molecular Probes) solution at 4°C overnight. Following overnight incubation, the slides were washed 3 x 5 minutes in 1x PBS and incubated in Alexa 568 secondary antibody (1:2000, A10037, Invitrogen) solution for at least 2 hours at room temperature and washed 3 x 5 minutes in 1x PBS. The slides were mounted using ProLong® Gold Antifade Mountant with DAPI (P36931, Molecular Probes). Fluorescence images were captured using a Zeiss Axioplan 2 microscope equipped with an AxioCam HRc camera.

Counting nuclei

Ten micrometer retinal sections were mounted as described under Fluorescence histochemistry, and the number of nuclei within a region with a width of 67 µm that was perpendicular to and covered both the outer and inner nuclear layers were counted. Nuclei in the outer and inner nuclear layers were counted separately. We analysed six images from each of the three animals (LAB4, LAB6, and GS). Bar graphs were generated and statistical analysis of the technical replicates (one-way ANOVA with Tukey's post hoc multiple comparison analysis) was performed in GraphPad Prism 7.

Autofluorescence

Retinal sections were washed, incubated in blocking solution, and mounted as described under Fluorescence histochemistry. The exposure times for the excitation at 488 nm and 568 nm were fixed for all images taken (150 ms and 80 ms, respectively). Outlines of the

retinal pigment epithelium (RPE), as well as adjacent background regions, were drawn using the polygon selection tool in ImageJ (v1.51, NIH), and the area and mean fluorescence intensity were measured. The mean intensity of the autofluorescence in the RPE was calculated by subtracting the background intensity from the adjacent regions. We analysed six images from each of the three individuals used in the fluorescence histochemistry. Bar graph generation and statistical analysis were performed as described under Counting nuclei.

Acknowledgements

The authors would like to thank the veterinary clinicians Berit Wallin-Håkansson, Ida Möller and Stuart Ellis for diagnosing and collecting samples, Anna Svensson and Kiran Kumar Jagarlamudi for technical assistance with western blotting, Mihaela Martis at the Swedish Bioinformatics Infrastructure Sweden at SciLifeLab for bioinformatics advice and Kerstin Lindblad-Toh for valuable comments of earlier versions of the manuscript. We would also like to acknowledge the support of the dedicated dog owners who allowed their dogs to take part in this study. The authors would like to acknowledge the support of the National Genomics Infrastructure (NGI) / Uppsala Genome Center and UPPMAX for providing computational infrastructure.

Funding

This study was funded by generous support by FORMAS, AGRIA and the Swedish Kennel Club research fund.

Author contributions

G.A. and T.B. conceived, designed and directed the study; B.E. and K.N. collected field material and diagnosed the subjects; B.E. and K.M. performed OCT, C.J.Z. performed histological analysis; C.M. and S.R. provided samples and genotypes; M.G., S.M. and D.H. performed sequencing; S.M. and M.G. performed sequence analyses and bioinformatics with support from A.V.; S.M. performed qPCR and western blotting; M.H. and F.H. performed and analyzed fluorescence histochemistry experiments; S.M., T.B. and G.A. were responsible for preparing of the manuscript with particular contributions from M.G., M.H., F.H., B.E. and C.M; all authors read and approved the final manuscript.

Competing financial interests

The authors declare that the research was conducted in the absence of any commercial or financial relationships that could be construed as a potential conflict of interest. A patent application has been filed by the following authors and inventors, TB, GA, BE and SM.

Figure captions

Fig 1. Retinal morphology and function in canine Stargardt disease. (A) The tapetal fundus of an affected dog. Black arrows indicate mottling (darker foci) and white arrows slight attenuation of the retinal blood vessels. **(B)** OCT images along the visual streak in age-matched unaffected dog (top), carrier (middle) and an affected dog (bottom). White arrows indicate where two images have been concatenated. A general neuroretinal thinning is visible in the affected retina (blue arrow) and includes patches of severe retinal atrophy (red arrow). **(C)** Histology of a normal canine retina and **(D)** histology of an affected retina, with red arrows indicating cone photoreceptors and black arrows indicated accumulation of lipofuscin in RPE. **(E)** Dark-adapted FERG in response to a bright flash (arrow) in an age-matched

unaffected dog (green), a carrier (blue tracing) and an affected dog (black). **(F)** Light-adapted cone transient responses and **(G)** cone flicker responses with FERG.

FERG = flash-electroretinography; RPE = retinal pigment epithelium; OS = outer segments; OLM = outer limiting membrane; ONL = outer nuclear layer.

Fig 2. Loss-of-function mutation in the canine *ABCA4* gene. (A) Sanger sequencing traces spanning positions Chr6:55,146,545-55,146,564 (Canfam3.1) in exon 28 of the *ABCA4* gene of a wild-type $ABCA4^{+/+}$ dog (top), a heterozygous $ABCA4^{+/-}$ dog (middle), and a homozygous $ABCA4^{-/-}$ dog (bottom). **(B)** Predicted structure of canine full-length ABCA4 protein, based on the proposed human structure[26], and the putative truncated product as a result of the premature stop codon at amino acid position 1,395. **(C)** Schematic representation of the region where the insertion of cytosine (C) is found showing the nucleotide and amino acid sequences of a full-length (top) and truncated (bottom) protein. **(D)** Predicted topological organization of ABCA4 and its domains with the insertion leading to a premature stop codon marked with an arrow. The topological organization is based on the proposed human topological organization[27, 28].

ECD1 = first extracellular domain; TMD1 = first membrane-spanning region; NBD1 = first nucleotide-binding domain; ECD2 = second extracellular domain; TMD2 = second membrane-spanning region; NBD2 = second nucleotide-binding domain.

Fig 3. Characterization of *ABCA4* mRNA expression and western blot analyses of ABCA4 protein levels in the canine retina. (A) Relative *ABCA4* mRNA expression levels by quantitative RT-PCR in three different regions in three dogs with different genotypes ($ABCA4^{+/+}$, $ABCA4^{+/-}$ and $ABCA4^{-/-}$), normalized to *GAPDH* expression. **(B)** Western blot

446 analyses of ABCA4 (above), GAPDH (middle), and RHO (below) protein levels in retinal
447 tissue.
448
449 **Fig 4. Fluorescence histochemistry of ABCA4, cone photoreceptors, and**
450 **autofluorescence in the canine retina. (A-C)** Fluorescence micrographs showing
451 ABCA4 expression (red), FITC-conjugated peanut agglutinin (PNA, green) and DAPI
452 nuclear staining (blue) in wild-type ($ABCA4^{+/+}$), heterozygous ($ABCA4^{+/-}$), and affected
453 ($ABCA4^{-/-}$) retinas. PNA labels cone photoreceptors. Autofluorescence, indicative of
454 lipofuscin accumulation, was seen in the $ABCA4^{-/-}$ RPE. **(D)** Bar graph with the average
455 number of DAPI-stained nuclei within a given region of the ONL and the INL. **(E-G)**
456 Fluorescence micrographs of RPE without immunohistochemistry show autofluorescence.
457 **(H)** Bar graph with background-corrected mean autofluorescence-intensity in the RPE. Note
458 the reduction of ABCA4-immunoreactivity, PNA binding, higher autofluorescence, and
459 fewer nuclei in the ONL in the $ABCA4^{-/-}$ compared to $ABCA4^{+/+}$ or $ABCA4^{+/-}$ retinas. All
460 scale bars = 50 µm; RPE = retinal pigment epithelium; ONL = outer nuclear layer; INL =
461 inner nuclear layer; Because there was only one individual per genotype, the statistics are
462 valid for the technical replicates. ANOVA with Tukey's post hoc test, n=6; $^{**}P < 0.01$;
463 $^{***}P < 0.001$; $^{****}P < 0.0001$; mean ± S.D.
464
465

466 References

467 1. Beltran WA, Cideciyan AV, Guziewicz KE, Iwabe S, Swider M, Scott EM, et al. Canine
468 retina has a primate fovea-like bouquet of cone photoreceptors which is affected by
469 inherited macular degenerations. PLoS One. 2014;9(3):e90390. Epub 2014/03/07. doi:
470 10.1371/journal.pone.0090390. PubMed PMID: 24599007; PubMed Central PMCID:
471 PMCPMC3944008.

2. Berger W, Kloeckener-Gruissem B, Neidhardt J. The molecular basis of human retinal and vitreoretinal diseases. Progress in Retinal and Eye Research. 2010;29(5):335-75. doi: https://doi.org/10.1016/j.preteyeres.2010.03.004.
3. den Hollander AI, Black A, Bennett J, Cremers FPM. Lighting a candle in the dark: advances in genetics and gene therapy of recessive retinal dystrophies. The Journal of Clinical Investigation. 2010;120(9):3042-53. doi: 10.1172/JCI42258. PubMed PMID: PMC2929718.
4. Miyadera K, Kato K, Aguirre-Hernandez J, Tokuriki T, Morimoto K, Busse C, et al. Phenotypic variation and genotype-phenotype discordance in canine cone-rod dystrophy with an RPGRIP1 mutation. Molecular vision. 2009;15:2287-305. Epub 2009/11/26. PubMed PMID: 19936303; PubMed Central PMCID: PMCPMC2779058.
5. Downs LM, Wallin-Håkansson B, Bergström T, Mellersh CS. A novel mutation in TTC8 is associated with progressive retinal atrophy in the golden retriever. Canine Genetics and Epidemiology. 2014;1:4. doi: 10.1186/2052-6687-1-4. PubMed PMID: PMC4574394.
6. Downs LM, Hitti R, Pregnolato S, Mellersh CS. Genetic screening for PRA-associated mutations in multiple dog breeds shows that PRA is heterogeneous within and between breeds. Vet Ophthalmol. 2014;17(2):126-30. Epub 2013/11/22. doi: 10.1111/vop.12122. PubMed PMID: 24255994.
7. Beltran WA. The use of canine models of inherited retinal degeneration to test novel therapeutic approaches. Veterinary ophthalmology. 2009;12(3):192-204. doi: 10.1111/j.1463-5224.2009.00694.x. PubMed PMID: PMC3193984.
8. Magnusson H. Uber Retinitis Pigmentosa and Konsanguinitat beim hunde. Archiv fuer vergleichende Ophthalmologie. 1911;2:147-63.
9. Miyadera K, Acland GM, Aguirre GD. Genetic and phenotypic variations of inherited retinal diseases in dogs: the power of within- and across-breed studies. Mammalian genome : official journal of the International Mammalian Genome Society. 2012;23(1-2):40-61. Epub 2011/11/09. doi: 10.1007/s00335-011-9361-3. PubMed PMID: 22065099; PubMed Central PMCID: PMCPMC3942498.
10. Acland GM, Aguirre GD, Ray J, Zhang Q, Aleman TS, Cideciyan AV, et al. Gene therapy restores vision in a canine model of childhood blindness. Nat Genet. 2001;28(1):92-5.
11. Petersen-Jones SM, Komaromy AM. Dog models for blinding inherited retinal dystrophies. Human gene therapy Clinical development. 2015;26(1):15-26. Epub 2015/02/12. doi: 10.1089/humc.2014.155. PubMed PMID: 25671556; PubMed Central PMCID: PMCPMC4442585.
12. Occelli LM, Schon C, Seeliger MW, Biel M, Michalakis S, Petersen-Jones S, et al. Gene Supplementation Rescues Rod Function and Preserves Photoreceptor and Retinal Morphology in Dogs, Leading the Way Towards Treating Human PDE6A-Retinitis Pigmentosa. Human gene therapy. 2017;28(12):1198-201. Epub 2017/12/08. doi: 10.1089/hum.2017.155. PubMed PMID: 29212382.
13. Acland GM, Aguirre GD, Bennett J, Aleman TS, Cideciyan AV, Bennicelli J, et al. Long-term restoration of rod and cone vision by single dose rAAV-mediated gene transfer to the retina in a canine model of childhood blindness. Mol Ther. 2005;12(6):1072-82. doi: 10.1016/j.ymthe.2005.08.008.
14. Narfstrom K, Katz ML, Bragadottir R, Seeliger M, Boulanger A, Redmond TM, et al. Functional and structural recovery of the retina after gene therapy in the RPE65 null mutation dog. Invest Ophthalmol Vis Sci. 2003;44(4):1663-72. Epub 2003/03/27. PubMed PMID: 12657607.

519 15. Beltran WA, Cideciyan AV, Iwabe S, Swider M, Kosyk MS, McDaid K, et al. Successful
520 arrest of photoreceptor and vision loss expands the therapeutic window of retinal gene
521 therapy to later stages of disease. Proceedings of the National Academy of Sciences.
522 2015;112(43):E5844-E53. doi: 10.1073/pnas.1509914112.
523 16. Mowat FM, Breuwer AR, Bartoe JT, Annear MJ, Zhang Z, Smith AJ, et al. RPE65 gene
524 therapy slows cone loss in Rpe65-deficient dogs. Gene Therapy. 2012;20(5):545-55. doi:
525 10.1038/gt.2012.63
526 https://www.nature.com/articles/gt201263#supplementary-information.
527 17. Zangerl B, Goldstein O, Philp AR, Lindauer SJP, Pearce-Kelling SE, Mullins RF, et al.
528 Identical Mutation in a Novel Retinal Gene Causes Progressive Rod-Cone Degeneration in
529 Dogs and Retinitis Pigmentosa in Man. Genomics. 2006;88(5):551-63. doi:
530 10.1016/j.ygeno.2006.07.007. PubMed PMID: PMC3989879.
531 18. RetNet. Retinal Information Network [cited 2018 29 Jan]. Available from:
532 https://sph.uth.tmc.edu/retnet/.
533 19. Mathur P, Yang J. Usher syndrome: Hearing loss, retinal degeneration and associated
534 abnormalities. Biochim Biophys Acta. 2015;1852(3):406-20. doi:
535 https://doi.org/10.1016/j.bbadis.2014.11.020.
536 20. Allikmets R, Singh N, Sun H, Shroyer NF, Hutchinson A, Chidambaram A, et al. A
537 photoreceptor cell-specific ATP-binding transporter gene (ABCR) is mutated in recessive
538 Stargardt macular dystrophy. Nat Genet. 1997;15(3):236-46. Epub 1997/03/01. doi:
539 10.1038/ng0397-236. PubMed PMID: 9054934.
540 21. Illing M, Molday LL, Molday RS. The 220-kDa rim protein of retinal rod outer
541 segments is a member of the ABC transporter superfamily. The Journal of biological
542 chemistry. 1997;272(15):10303-10. Epub 1997/04/11. PubMed PMID: 9092582.
543 22. Papermaster DS, Schneider BG, Zorn MA, Kraehenbuhl JP. Immunocytochemical
544 localization of a large intrinsic membrane protein to the incisures and margins of frog rod
545 outer segment disks. The Journal of cell biology. 1978;78(2):415-25. Epub 1978/08/01.
546 PubMed PMID: 690173; PubMed Central PMCID: PMCPMC2110123.
547 23. Sun H, Nathans J. Stargardt's ABCR is localized to the disc membrane of retinal rod
548 outer segments. Nat Genet. 1997;17(1):15-6. Epub 1997/09/01. doi: 10.1038/ng0997-15.
549 PubMed PMID: 9288089.
550 24. Quazi F, Molday RS. ATP-binding cassette transporter ABCA4 and chemical
551 isomerization protect photoreceptor cells from the toxic accumulation of excess 11-cis-
552 retinal. Proc Natl Acad Sci U S A. 2014;111(13):5024-9. Epub 2014/04/08. doi:
553 10.1073/pnas.1400780111. PubMed PMID: 24707049; PubMed Central PMCID:
554 PMCPMC3977269.
555 25. Lykke-Andersen S, Jensen TH. Nonsense-mediated mRNA decay: an intricate
556 machinery that shapes transcriptomes. Nature reviews Molecular cell biology.
557 2015;16(11):665-77. doi: 10.1038/nrm4063
558 https://www.nature.com/articles/nrm4063#supplementary-information.
559 26. Tsybovsky Y, Molday RS, Palczewski K. The ATP-binding cassette transporter ABCA4:
560 structural and functional properties and role in retinal disease. Advances in experimental
561 medicine and biology. 2010;703:105-25. Epub 2010/08/17. doi: 10.1007/978-1-4419-5635-
562 4_8. PubMed PMID: 20711710; PubMed Central PMCID: PMCPMC2930353.
563 27. Bungert S, Molday LL, Molday RS. Membrane Topology of the ATP Binding Cassette
564 Transporter ABCR and Its Relationship to ABC1 and Related ABCA Transporters:

identification of N-linked glycosylation sites. The Journal of biological chemistry. 2001;276(26):23539-46. doi: 10.1074/jbc.M101902200.

28. Biswas-Fiss EE, Affet S, Ha M, Biswas SB. Retinoid binding properties of nucleotide binding domain 1 of the Stargardt disease-associated ATP binding cassette (ABC) transporter, ABCA4. The Journal of biological chemistry. 2012;287(53):44097-107. Epub 2012/11/13. doi: 10.1074/jbc.M112.409623. PubMed PMID: 23144455; PubMed Central PMCID: PMCPMC3531725.

29. Damiani D, Alexander JJ, O'Rourke JR, McManus M, Jadhav AP, Cepko CL, et al. Dicer inactivation leads to progressive functional and structural degeneration of the mouse retina. J Neurosci. 2008;28(19):4878-87. Epub 2008/05/09. doi: 10.1523/jneurosci.0828-08.2008. PubMed PMID: 18463241; PubMed Central PMCID: PMCPMC3325486.

30. Delori FC, Staurenghi G, Arend O, Dorey CK, Goger DG, Weiter JJ. In vivo measurement of lipofuscin in Stargardt's disease - Fundus flavimaculatus. Invest Ophthalmol Vis Sci. 1995;36(11):2327-31. Epub 1995/10/01. PubMed PMID: 7558729.

31. Molday LL, Rabin AR, Molday RS. ABCR expression in foveal cone photoreceptors and its role in Stargardt macular dystrophy. Nat Genet. 2000;25(3):257-8. Epub 2000/07/11. doi: 10.1038/77004. PubMed PMID: 10888868.

32. Quazi F, Lenevich S, Molday RS. ABCA4 is an N-retinylidene-phosphatidylethanolamine and phosphatidylethanolamine importer. Nature communications. 2012;3(925):1-9. Epub 2012/06/28. doi: 10.1038/ncomms1927. PubMed PMID: 22735453; PubMed Central PMCID: PMCPMC3871175.

33. Kiser PD, Golczak M, Palczewski K. Chemistry of the Retinoid (Visual) Cycle. Chem Rev. 2014;114(1):194-232. doi: 10.1021/cr400107q. PubMed PMID: PMC3858459.

34. Mata NL, Weng J, Travis GH. Biosynthesis of a major lipofuscin fluorophore in mice and humans with ABCR-mediated retinal and macular degeneration. Proc Natl Acad Sci U S A. 2000;97(13):7154-9. PubMed PMID: PMC16515.

35. Weng J, Mata NL, Azarian SM, Tzekov RT, Birch DG, Travis GH. Insights into the function of Rim protein in photoreceptors and etiology of Stargardt's disease from the phenotype in abcr knockout mice. Cell. 1999;98(1):13-23. Epub 1999/07/21. doi: 10.1016/s0092-8674(00)80602-9. PubMed PMID: 10412977.

36. Young RW. The renewal of photoreceptor cell outer segments. The Journal of cell biology. 1967;33(1):61-72. PubMed PMID: PMC2107286.

37. Young RW, Bok D. Participation of the retinal pigment epithelium in the rod outer segment renewal process. The Journal of cell biology. 1969;42(2):392-403. PubMed PMID: PMC2107669.

38. Eldred GE, Lasky MR. Retinal age pigments generated by self-assembling lysosomotropic detergents. Nature. 1993;361(6414):724-6. doi: 10.1038/361724a0.

39. Ben-Shabat S, Parish CA, Vollmer HR, Itagaki Y, Fishkin N, Nakanishi K, et al. Biosynthetic Studies of A2E, a Major Fluorophore of Retinal Pigment Epithelial Lipofuscin. The Journal of biological chemistry. 2002;277(9):7183-90. doi: 10.1074/jbc.M108981200.

40. Ng KP, Gugiu B, Renganathan K, Davies MW, Gu X, Crabb JS, et al. Retinal pigment epithelium lipofuscin proteomics. Molecular & cellular proteomics : MCP. 2008;7(7):1397-405. Epub 2008/04/26. doi: 10.1074/mcp.M700525-MCP200. PubMed PMID: 18436525; PubMed Central PMCID: PMCPMC2493379.

41. Strauss O. The Retinal Pigment Epithelium in Visual Function. Physiol Rev. 2005;85(3):845-81. doi: 10.1152/physrev.00021.2004. PubMed PMID: 15987797.

611 42. Cideciyan AV, Swider M, Aleman TS, Roman MI, Sumaroka A, Schwartz SB, et al.
612 Reduced-illuminance autofluorescence imaging in ABCA4-associated retinal degenerations.
613 Journal of the Optical Society of America A, Optics, image science, and vision.
614 2007;24(5):1457-67. Epub 2007/04/13. PubMed PMID: 17429493; PubMed Central PMCID:
615 PMCPMC2579898.
616 43. Cremers FP, van de Pol DJ, van Driel M, den Hollander AI, van Haren FJ, Knoers NV, et
617 al. Autosomal recessive retinitis pigmentosa and cone-rod dystrophy caused by splice site
618 mutations in the Stargardt's disease gene ABCR. Hum Mol Genet. 1998;7(3):355-62. Epub
619 1998/04/18. PubMed PMID: 9466990.
620 44. Maugeri A, Klevering BJ, Rohrschneider K, Blankenagel A, Brunner HG, Deutman AF,
621 et al. Mutations in the ABCA4 (ABCR) Gene Are the Major Cause of Autosomal Recessive
622 Cone-Rod Dystrophy. Am J Hum Genet. 2000;67(4):960-6. PubMed PMID: PMC1287897.
623 45. Martinez-Mir A, Paloma E, Allikmets R, Ayuso C, del Rio T, Dean M, et al. Retinitis
624 pigmentosa caused by a homozygous mutation in the Stargardt disease gene ABCR. Nat
625 Genet. 1998;18(1):11-2. Epub 1998/01/13. doi: 10.1038/ng0198-11. PubMed PMID:
626 9425888.
627 46. Lek M, Karczewski KJ, Minikel EV, Samocha KE, Banks E, Fennell T, et al. Analysis of
628 protein-coding genetic variation in 60,706 humans. Nature. 2016;536(7616):285-91. doi:
629 10.1038/nature19057
630 https://www.nature.com/articles/nature19057#supplementary-information.
631 47. ExAC Browser. Exome Aggregation Consortium [cited 2018 29 Jan]. Available from:
632 http://exac.broadinstitute.org.
633 48. Nasonkin I, Illing M, Koehler MR, Schmid M, Molday RS, Weber BH. Mapping of the
634 rod photoreceptor ABC transporter (ABCR) to 1p21-p22.1 and identification of novel
635 mutations in Stargardt's disease. Human genetics. 1998;102(1):21-6. Epub 1998/03/07.
636 PubMed PMID: 9490294.
637 49. Rozet JM, Gerber S, Souied E, Perrault I, Chatelin S, Ghazi I, et al. Spectrum of ABCR
638 gene mutations in autosomal recessive macular dystrophies. European journal of human
639 genetics : EJHG. 1998;6(3):291-5. Epub 1998/10/22. doi: 10.1038/sj.ejhg.5200221. PubMed
640 PMID: 9781034.
641 50. Stone EM, Webster AR, Vandenburgh K, Streb LM, Hockey RR, Lotery AJ, et al. Allelic
642 variation in ABCR associated with Stargardt disease but not age-related macular
643 degeneration. Nat Genet. 1998;20(4):328-9. doi: 10.1038/3798.
644 51. Lu LJ, Liu J, Adelman RA. Novel therapeutics for Stargardt disease. Graefes Arch Clin
645 Exp Ophthalmol. 2017;255(6):1057-62. doi: 10.1007/s00417-017-3619-8.
646 52. Auricchio A, Trapani I, Allikmets R. Gene Therapy of ABCA4-Associated Diseases. Cold
647 Spring Harb Perspect Med. 2015;5(5):a017301. doi: 10.1101/cshperspect.a017301. PubMed
648 PMID: PMC4448589.
649 53. Tanna P, Strauss RW, Fujinami K, Michaelides M. Stargardt disease: clinical features,
650 molecular genetics, animal models and therapeutic options. Br J Ophthalmol.
651 2017;101(1):25-30. doi: 10.1136/bjophthalmol-2016-308823. PubMed PMID: PMC5256119.
652 54. Marmorstein AD, Marmorstein LY. The challenge of modeling macular degeneration
653 in mice. Trends Genet. 2007;23(5):225-31. doi: https://doi.org/10.1016/j.tig.2007.03.001.
654 55. Pichard V, Provost N, Mendes-Madeira A, Libeau L, Hulin P, Tshilenge K-T, et al. AAV-
655 mediated Gene Therapy Halts Retinal Degeneration in PDE6β-deficient Dogs. Mol Ther.
656 2016;24(5):867-76. doi: https://doi.org/10.1038/mt.2016.37.

56. Zangerl B, Lindauer SJ, Acland GM, Aguirre GD. Identification of genetic variation and haplotype structure of the canine ABCA4 gene for retinal disease association studies. Mol Genet Genomics. 2010;284(4):243-50. doi: 10.1007/s00438-010-0560-5. PubMed PMID: PMC2954605.

57. Lippmann T, Pasternack SM, Kraczyk B, Dudek SE, Dekomien G. Indirect exclusion of four candidate genes for generalized progressive retinal atrophy in several breeds of dogs. Journal of negative results in biomedicine. 2006;5:19. Epub 2006/12/01. doi: 10.1186/1477-5751-5-19. PubMed PMID: 17134500; PubMed Central PMCID: PMCPMC1716180.

58. Kijas JW, Zangerl B, Miller B, Nelson J, Kirkness EF, Aguirre GD, et al. Cloning of the canine ABCA4 gene and evaluation in canine cone-rod dystrophies and progressive retinal atrophies. Molecular vision. 2004;10:223-32. Epub 2004/04/06. PubMed PMID: 15064680.

59. Karlstam L, Hertil E, Zeiss C, Ropstad EO, Bjerkås E, Dubielzig RR, et al. A slowly progressive retinopathy in the Shetland Sheepdog. Vet Ophthalmol. 2011;14(4):227-38. doi: doi:10.1111/j.1463-5224.2010.00866.x.

60. Ekesten B, Komáromy AM, Ofri R, Petersen-Jones SM, Narfström K. Guidelines for clinical electroretinography in the dog: 2012 update. Doc Ophthalmol. 2013;127(2):79-87. doi: 10.1007/s10633-013-9388-8.

61. Bolger AM, Lohse M, Usadel B. Trimmomatic: a flexible trimmer for Illumina sequence data. Bioinformatics. 2014;30(15):2114-20. doi: 10.1093/bioinformatics/btu170. PubMed PMID: PMC4103590.

62. Li H, Durbin R. Fast and accurate short read alignment with Burrows–Wheeler transform. Bioinformatics. 2009;25(14):1754-60. doi: 10.1093/bioinformatics/btp324. PubMed PMID: PMC2705234.

63. Li H, Handsaker B, Wysoker A, Fennell T, Ruan J, Homer N, et al. The Sequence Alignment/Map format and SAMtools. Bioinformatics. 2009;25(16):2078-9. Epub 2009/06/10. doi: 10.1093/bioinformatics/btp352. PubMed PMID: 19505943; PubMed Central PMCID: PMCPMC2723002.

64. McKenna A, Hanna M, Banks E, Sivachenko A, Cibulskis K, Kernytsky A, et al. The Genome Analysis Toolkit: a MapReduce framework for analyzing next-generation DNA sequencing data. Genome research. 2010;20(9):1297-303. Epub 2010/07/21. doi: 10.1101/gr.107524.110. PubMed PMID: 20644199; PubMed Central PMCID: PMCPMC2928508.

65. DePristo MA, Banks E, Poplin R, Garimella KV, Maguire JR, Hartl C, et al. A framework for variation discovery and genotyping using next-generation DNA sequencing data. Nat Genet. 2011;43(5):491-8. Epub 2011/04/12. doi: 10.1038/ng.806. PubMed PMID: 21478889; PubMed Central PMCID: PMCPMC3083463.

66. Wang K, Li M, Hakonarson H. ANNOVAR: functional annotation of genetic variants from high-throughput sequencing data. Nucleic acids research. 2010;38(16):e164. Epub 2010/07/06. doi: 10.1093/nar/gkq603. PubMed PMID: 20601685; PubMed Central PMCID: PMCPMC2938201.

67. Adzhubei IA, Schmidt S, Peshkin L, Ramensky VE, Gerasimova A, Bork P, et al. A method and server for predicting damaging missense mutations. Nat Methods. 2010;7(4):248-9. Epub 2010/04/01. doi: 10.1038/nmeth0410-248. PubMed PMID: 20354512; PubMed Central PMCID: PMCPMC2855889.

68. Choi Y, Sims GE, Murphy S, Miller JR, Chan AP. Predicting the functional effect of amino acid substitutions and indels. PLoS One. 2012;7(10):e46688. Epub 2012/10/12. doi:

10.1371/journal.pone.0046688. PubMed PMID: 23056405; PubMed Central PMCID: PMCPMC3466303.

69. Robinson JT, Thorvaldsdóttir H, Winckler W, Guttman M, Lander ES, Getz G, et al. Integrative genomics viewer. Nature Biotechnology. 2011;29:24. doi: 10.1038/nbt.1754 https://www.nature.com/articles/nbt.1754#supplementary-information.

70. Thorvaldsdóttir H, Robinson JT, Mesirov JP. Integrative Genomics Viewer (IGV): high-performance genomics data visualization and exploration. Briefings in Bioinformatics. 2013;14(2):178-92. doi: 10.1093/bib/bbs017.

71. Koressaar T, Remm M. Enhancements and modifications of primer design program Primer3. Bioinformatics. 2007;23(10):1289-91. Epub 2007/03/24. doi: 10.1093/bioinformatics/btm091. PubMed PMID: 17379693.

72. Untergasser A, Cutcutache I, Koressaar T, Ye J, Faircloth BC, Remm M, et al. Primer3—new capabilities and interfaces. Nucleic acids research. 2012;40(15):e115-e. doi: 10.1093/nar/gks596. PubMed PMID: PMC3424584.

Supporting information

S1 Fig. Pedigree of the Labrador retriever dogs used in the study. Filled symbols indicate affected individuals, half-filled symbols represent obligate or genotyped carriers of the *ABCA4* insertion. Individuals LAB1 to LAB4 were used in the WGS analysis. Numbered individuals were genotyped for the insertion in the *ABCA4* gene (c.4176insC) and for the non-synonymous substitution in the *USH2A* gene (c.7244C>T). In addition, five unrelated, unaffected dogs (not shown in the figure) were genotyped and found to be either wild-type or heterozygous for the variants in the *ABCA4* and the *USH2A* gene (LAB21 to LAB25). Crosses intersecting the dashed lines indicate the number of generations between the individuals.

S1 Table. Summary of the whole-genome sequencing runs 1 and 2.

S2 Table. Exonic variants identified in WGS. Number of exonic variants following autosomal recessive inheritance pattern (AR) in Trio1 and Trio2, each consisting of the parents and one of the two offspring. The total number of exonic variants in the family quartet including all inheritance patterns and the number of AR variants shared between the two trios. The "unique" column represents the number of AR variants, which were shared

735 between the two trios and not found to be homozygous in 23 additional investigated canine
736 genome sequences.

737 **S3 Table. List of candidate variants from WGS.** Coding sequence variants identified as
738 private for the Labrador retriever family and the predicted effect of the variants based on
739 Polyphen-2 and PROVEAN scores.

740 **S4 Table. Validation of variants c.4176insC in ABCA4 gene and c.C7244T in USH2A**
741 **gene by Sanger sequencing.**

742 **S5 Table. Canine primer sequences used in the analysis.**

743

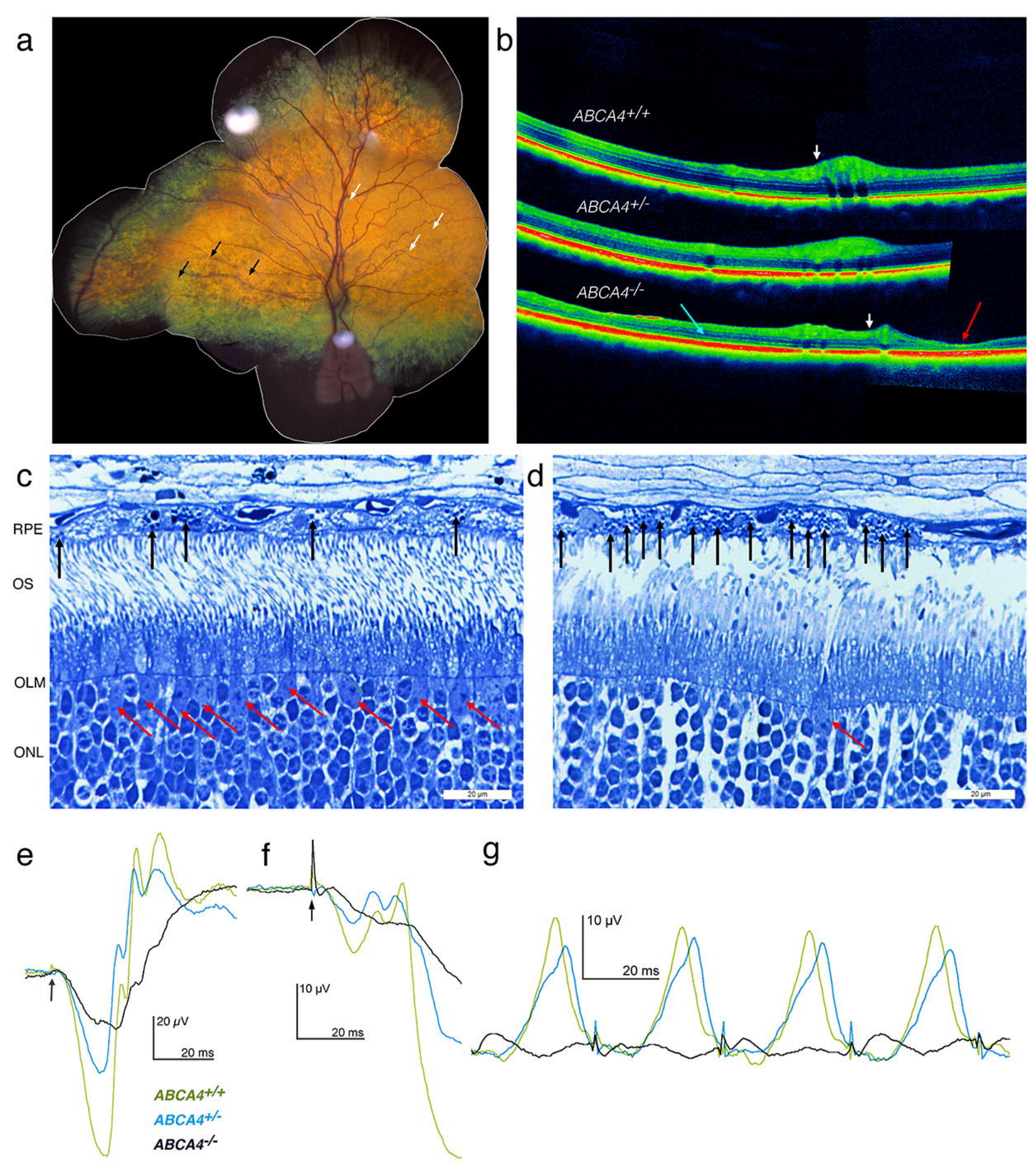
a
b
ABCA4+/+
ABCA4+/-
ABCA4-/-
c
d
RPE
OS
OLM
ONL
20 µm
20 µm
e
f
g
20 µV
20 ms
10 µV
20 ms
10 µV
20 ms
ABCA4+/+
ABCA4+/-
ABCA4-/-